Since January 2020 Elsevier has created a COVID-19 resource centre with free information in English and Mandarin on the novel coronavirus COVID-19. The COVID-19 resource centre is hosted on Elsevier Connect, the company's public news and information website.

Elsevier hereby grants permission to make all its COVID-19-related research that is available on the COVID-19 resource centre - including this research content - immediately available in PubMed Central and other publicly funded repositories, such as the WHO COVID database with rights for unrestricted research re-use and analyses in any form or by any means with acknowledgement of the original source. These permissions are granted for free by Elsevier for as long as the COVID-19 resource centre remains active.

journal of the mechanical behavior of biomedical materials 135 (2022) 105406

Contents lists available at ScienceDirect

Journal of the Mechanical Behavior of Biomedical Materials

journal homepage: www.elsevier.com/locate/jmbbm

Modal analysis of novel coronavirus (SARS COV-2) using finite element methodology

Caaisha Warsame [a], Daniele Valerini [b], Iñigo Llavori [c], Asa H. Barber [a], Saurav Goel [a,d,*]

[a] School of Engineering, London South Bank University, 103 Borough Road, London, SE1 0AA, UK
[b] SSPT-PROMAS-MATAS, ENEA – Italian National Agency for New Technologies, Energy and Sustainable Economic Development, S.S. 7 Appia, km 706, 72100, Brindisi, Italy
[c] Faculty of Engineering, Mondragon Unibertsitatea, 20500, Arrasate, Gipuzkoa, Spain
[d] Department of Mechanical Engineering, University of Petroleum and Energy Studies, Dehradun, 248007, India

ARTICLE INFO

Keywords:
Modal analysis
SARS-CoV-2
COVID-19
Finite element analysis (FEA)
Natural frequencies

ABSTRACT

Many new engineering and scientific innovations have been proposed to date to passivate the novel coronavirus (SARS CoV-2), with the aim of curing the related disease that is now recognised as COVID-19. Currently, vaccine development remains the most reliable solution available. Efforts to provide solutions as alternatives to vaccinations are growing and include established control of behaviours such as self-isolation, social distancing, employing facial masks and use of antimicrobial surfaces. The work here proposes a novel engineering method employing the concept of resonant frequencies to denature SARS CoV-2. Specifically, "modal analysis" is used to computationally analyse the Eigenvalues and Eigenvectors i.e. frequencies and mode shapes to denature COVID-19. An average virion dimension of 63 nm with spike proteins number 6, 7 and 8 were examined, which revealed a natural frequency of a single virus in the range of 88–125 MHz. The information derived about the natural frequency of the virus through this study will open newer ways to exploit medical solutions to combat future pandemics.

1. Introduction

The recently identified pathogen "Severe Acute Respiratory Syndrome Coronavirus 2 (SARS CoV-2)", resulting in the Coronavirus Disease COVID-19, has caused a significant worldwide impact. Demands for effective methods and innovations that can tackle the COVID-19 pandemic are therefore considerable. Any approach must first consider the features of the disease to develop suitable treatments. A recent review (Goel et al., 2020) revealed that the SARS CoV-2 structure (see Fig. 1(a)) comprises of spike proteins, envelope protein and membrane protein, surrounding the genomic RNA.

A typical spike protein has an approximate unit mass of 180–200 kDa and a length of 1273 amino acids (Huang et al., 2020). The SARS CoV-2 envelope is an important element that plays a major role in the replication of SARS-CoV-2 (Kiss et al., 2021) (Arbely et al., 2004) (Raamsman et al., 2000). The helical shape of the virus envelope depends on the size of the nucleic acid, the membrane proteins modulate the maturation and retention of the spike protein allowing the assembly of virus-like particles. The nucleocapsid protein is responsible for the viral replication cycle, as well as the cellular response of host cell to viral infection and processes regarding the viral genome (Venkatagopalan et al., 2015) (Tai et al., 2020) (Jiang et al., 2020).

Despite the benefits provided by the development of vaccines and short-term measures such as social distancing, face masks, self-isolation and disinfection, no immediate solution to prevent the spreading of the virus have been discovered yet. Vaccine development is a time-consuming activity that requires field trials before being made available for use. Moreover, vaccine is only effective against specific disease for which it is developed, potentially requiring new vaccines for future pandemics, and the vaccine efficacy reduces over time due to the antimicrobial resistance (AMR).

This study proposes a novel holistic view to denature SARS-CoV-2 or any other microbe by applying resonant natural frequencies using an external apparatus. The motivation of this paper is to investigate this hypothesis numerically and to evaluate the range of frequencies required to denature SARS-CoV-2. The necessary mechanical properties of SARS-CoV-2 such as its density (ρ), Young's modulus (E) and Poisson's ratio (ν), were obtained from prior literature data (Yao and Wang, 2020) (Ivanovska et al., 2004) (Tachibana et al., 2004). In this novel

* Corresponding author. School of Engineering, London South Bank University, 103 Borough Road, London, SE1 0AA, UK.
E-mail address: goels@lsbu.ac.uk (S. Goel).

https://doi.org/10.1016/j.jmbbm.2022.105406
Received 30 May 2022; Received in revised form 11 July 2022; Accepted 26 July 2022
Available online 20 August 2022
1751-6161/© 2022 The Authors. Published by Elsevier Ltd. This is an open access article under the CC BY license (http://creativecommons.org/licenses/by/4.0/).

Abbreviations

$\ddot{x}$	Acceleration vector
$\dot{x}$	Velocity vector
x	Displacement vector
u	Mode shape matrix
x_0	Initial deflection
q_i	Modal coordinate for nth number

study, we attempt to simulate the entire virus structure as opposed to simulating a single spike protein previously shown by (Yao and Wang, 2020). Moreover, by doing so, we were able to use the experimental data gathered from atomic force microscopy (AFM) (Kiss et al., 2021) to evaluate the dynamic response analyses (Yao and Wang, 2020). This new knowledge will foster rapid advances in biomedical research to non-invasively destroy microbes in a sustainable way without involving the use of chemicals, thus helping to address the growing concern of antimicrobial resistance (AMR).

2. Literature review

In the published literature, there is unique evidence where an AFM nanoindentation was used to induce topographical changes in the structure of SARS-CoV-2 virion (Kiss et al., 2021). This experimental study aimed to gather information about the forces required to induce inelastic deformation in the virion. A Ø 80 nm diameter SARS CoV-2 virion was penetrated repeatedly using an AFM tip until the peripheral top wall touched the bottom wall of the virion. Surprisingly, the virion did not fracture and an anomalous large elastic behaviour was observed during this AFM indentation study (Sally, 2020). (Kiss et al., 2021) concluded that SARS CoV-2 has high self-healing ability and possesses vastly abnormal elasticity.

(Wierzbicki et al., 2021) conducted a study by looking at the effect of the receptors (spikes) of the coronavirus family from the point of view of rigorous laws of continuum mechanics and structural dynamics. The objective of the work was to identify the most probable damage scenario of the family of coronaviruses, subjected to harmonic excitation. The paper used simple concept of the mechanics and physics of solids and lacks the incorporation of geometry and material properties of the virus. Moreover, it is known that a virus does not make an exact copy of itself in the reproduction cycle. In the coronavirus family, the size, shape, and distribution of the receptors (spikes) vary considerably across the surface of the virus and from one virus to the other (Neuman Benjamin et al., 2006). In literature, it was reported by numerous studies that the numbers of spikes differed from one another; for SARS-CoV-2 an average of 61 spikes were reported by (Kiss et al., 2021), 24 by (Ke et al., 2020), 30 by (Yao and Wang, 2020) and 40 by (Turoňová et al., 2020). Wierzbicki et al. (2021) considered a total of 96 spikes as they validated their study by comparing a TGEV pig virus where the total height of the spike was 16 nm and the lipid bilayer (a thin elastic shell with radius to thickness ratio of 1.25) was of intermediate thickness. The single degree-of-freedom model they developed predicted the resonant vibration of single spike to be about 112 MHz, which was close to the finite element analysis (FEA) estimated value of 110 MHz.

In addition, Dastjerdi et al. (2022) evaluated the natural frequency of SARS-CoV-2 cells using Eringen's nonlocal elasticity theory. This study applied the shell theory of structures and considered the body of virus as a spherical structure. The natural frequencies of the SARS-CoV-2 virus were obtained using the dynamic equations. The virus was modelled by considering parameters needed from the governing equation of a spherical structure. The study by (Dastjerdi et al., 2022) considered a linear elastic spring model and reported the natural frequencies for various radii of the SARS-CoV-2 virus (50, 80, 100, 120 and 150 nm). Considering a common SARS-CoV-2 radius of about 100 nm, Dastjerdi et al. (2022) found the first natural frequency to be in the range of 3 GHz $< f <$ 4 GHz and the second in the range 7 GHz $< f <$ 25 GHz. However, it is widely known that viruses differ in size and shape from one another. Consequently, the shape and size of the virus as well as the distribution of the spikes can be influential in establishing the natural frequency of a given virus (Neuman Benjamin et al., 2006).

(Yao and Wang, 2020) used FEA approach to study the modal characteristics of a single spike protein for tuned (all spike proteins being identical) and mistuned 2019-nCoV model in fluid, representing human blood. The first 200 frequencies for the tuned 2019-nCoV model found by them as first-order bending vibrations were similar to each other in the range of 190 MHz–200 MHz. This study considered a fixed size virion of 200 nm to mimic 2019-nCoV virus. Prior studies shows that the physical size of SARS-CoV-2 can vary considerably from approximately 45 to 140 nm (Lyonnais et al., 2021). Similarly, different numbers of spikes proteins were reported in the literature such as an average of 61 spikes reported by (Kiss et al., 2021), 24 by (Ke et al., 2020), 30 by (Yao and Wang, 2020) and 40 by (Turoňová et al., 2020). This implies that the number of spike proteins varies depending on the age of the virion (Kiss et al., 2021). In our model development of the SARS CoV-2 virus, we have considered the data reported by (Lyonnais et al., 2021). We constructed the virus assuming a diameter of 63 nm and taking the number of spike proteins as 6, 7 and 8 respectively. In this

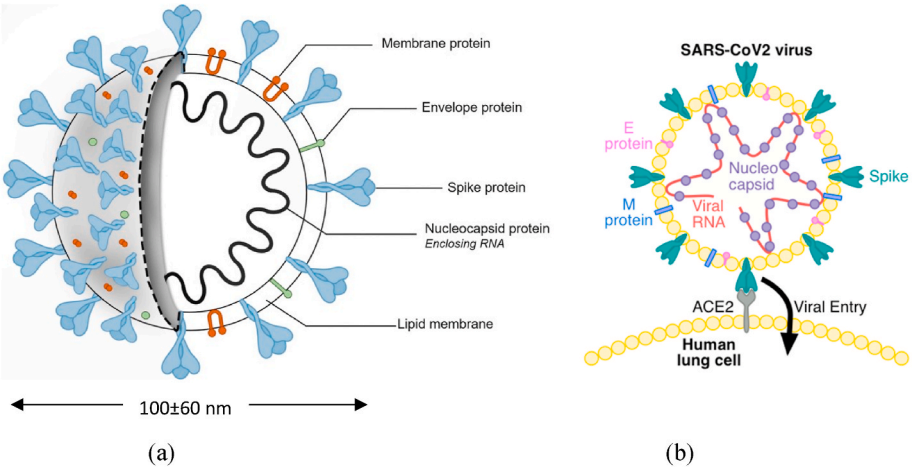

Fig. 1. Illustration of SARS-CoV-2 showing (a) Anatomy of SARS CoV-2 and (b) likely mechanism of infection, showing Envelope (E) Protein, Membrane (M) Protein, Spike (S) Protein, Nucleocapsid (N) Protein (blue dots) and genomic RNA (red chain) (Goel et al., 2020).

aspect, Table 1 shows the physical properties of SARS-CoV-2 derived from the literature which were used as input for the FEA model.

As such, this novel work on modal analysis of novel coronavirus (SARS COV-2) using finite element methodology provides a deep insight into the resonant frequency of SARS CoV-2 by performing the analysis on different spike proteins numbers using similar virion size, as well as using an approach of using the modal analysis technique to examine the natural frequencies of the whole virus model as opposed to investigating the natural frequencies of a single spike protein by (Yao and Wang, 2020). A maximum of 100 eigenvalues were computed, and the last 7 values were extracted to perform a mesh convergence study to establish the frequencies most likely to fail the virus structurally. From this analysis, recommendations were drawn for the future experimental works to develop an apparatus that can use the theoretical knowledge developed in this work to efficiently design the device.

3. Experimental setup and methodology

Fig. 2 presents a schematic diagram of the SARS-CoV-2 modal analysis model developed in this paper. The preliminary setup consisted of mainly identifying the correct parameters needed to feed the simulation model, such as density and elasticity, specifically Young's modulus and Poisson ratio (Kiss et al., 2021) (Stephanidis et al., 2007) (Ivanovska et al., 2004) (Tachibana et al., 2004) (Abaqus, 2012), as reported in Table 1. In the study by (Yao and Wang, 2020), it was reported that it is essential to use the nonlocal elasticity theory to consider the size effect of nanomaterials. However, in prior studies performed by (Peddieson et al., 2003) on a cantilever under concentrated force, its bending behaviour revealed using nonlocal elasticity theory showed similar results to that of local results. Also (Kiss et al., 2021), found that when a cantilever tip was lowered on the vertex of an individual SARS-CoV-2 virion, the nanomechanical manipulation did not result in permanent topographical changes in spite of completely compressing the virion. They observed a linear force response and that the elastic regime followed with a yield point marking the deviation from the linear force response and the onset of force-induced structural transition. These literature evidence suggests that the classical elastic theory is applicable to investigate the modal analysis of SARS CoV-2 using FEA. Accordingly, a commercial software Abaqus/CAE was used to assign the model with a category of type solid homogenous based on the properties identified in the parameters. The category type solid homogenous was chosen because the model is a three-dimensional region, with no thickness and a solid without a hollow part. A step was then created by using the linear perturbation state and then modal analysis was performed. The analyses of data revealed 7, 21 and 100 eigenvalues (Abaqus, 2012). These eigenvalues were chosen due to close proximity to one another amongst the 100 eigenvalues to compare at which frequency range the mesh convergence error would be at its minimum. As for the load, 6, 7 and 8 boundary conditions were fixed to the models to anchor the virus movement when it is attached to the receptor site on the host cell membrane. It is unlikely for a single spike protein to be attached to a cell when it is in contact. Hence, 6, 7 and 8 fixed spike proteins were chosen to evaluate the natural frequencies of the SARS-CoV-2 model. These fixed spike proteins represented a cantilever section such that the type of chosen step was Symmetry/Antisymmetry/Encastre and the encastre selected was of (U1=U2=U3=UR1 = UR2 = UR3 = 0) (Mia et al., 2017) The model was then meshed with a seed part of 1.5, element shape tetrahedron, technique free, element library standard, geometric order linear and lastly to create a job which submits the model file to Abaqus to run the simulation using implicit solver. A mesh convergence study was later conducted for the last 7 values of the 7, 21 and 100 eigenvalues and frequencies.

Table 1
Physical properties of SARS-CoV-2 gathered from various sources including Kiss et al. (2021).

Spherical mean diameter	62 nm (±8 nm, S.D.)
Mean distance between the spike trimers	21 nm (±6 nm, S.D.)
Mean height of the spike trimers	13 nm (±5 nm, S.D.)
Number of spike proteins	61
Mean virion stiffness	13 pN/nm (±5 pN/nm, S.D.)
Thermal denaturation	90 °C
Unfolding force of the S protein	210–330 pN
Mass	10^3 MDa = $1.6605x10^{-18}$ kg
Volume	10^6 nm^3 = $1x10^{-21}$ m^3
Density	$1.66x10^3$ Kg/m^3
Elasticity	$1.24\ x\ 10^{-13}$ N/m^2
Poisson's ratio	0.3

4. Result & discussions

A total of 100 eigenvalues for the SARS-CoV-2 structure were computed and the last 7 values were extracted to perform a mesh convergence to determine the set of most accurate frequencies. These requested eigenvalues were chosen due to their values being in close proximity to one another amongst the 100 eigenvalues. The procedure followed was unchanged for all the models assuming a fixed point of 6, 7 and 8 fixed spike proteins.

4.1. Frequency response of 63 nm virion diameter having 6 fixed spike proteins

Fig. 3 shows a range of virus configurations with variable fixed spike proteins for the virion with a central height of 63 nm. The frequencies gathered from the simulations were analysed to find which set of frequencies converged using equation (1) to establish errors between the requested eigenvalues of 7, 21 and 100.

$$Mesh\ Convergence\ error\ \% = \frac{j^{th}\ result - i^{th}\ result}{j^{th}\ result} \quad (1)$$

where j^{th} represent the last value and i^{th} represent the first value of the table for each eigenvalue of 7, 21 and 100 based on table 2, 3 and 4.

Fig. 3(a) shows 6 fixed spike proteins of the virion with a central height of 63 nm. As shown in Table 2 (Appendix 1), based on the mesh convergence error in the first set were approximately 34%, followed by the second set of frequency error of 0.01% and the last set showing an error of 2.17%. These results demonstrated that the second set of the frequencies had closer proximity compared to the first and third, and this indicated that the frequency set found in the model had met resonance.

4.2. Frequency response of 63 nm virion diameter having 7 fixed spike proteins

Fig. 3(b) shows 7 fixed spike proteins for the virion with a central height of 63 nm. As shown in Table 3 (Appendix 2), the mesh convergence error in the first set were 59%, followed by the second set of error of 0.09% and the last set of error of 11.31%. These results show that the second set of the frequencies had the lowest error (0.09%) in mesh convergence, and this suggests that the frequency set met the resonance.

4.3. Frequency response of 63 nm virion diameter having 8 fixed spike proteins

Fig. 3(c) shows 8 fixed spike proteins of the virion with a central height of 63 nm. As shown in Table 4 (Appendix 3), the mesh convergence error in the first set was 38%, followed by the second set of frequency error of 0.02% and the last set of frequency error was about 2.25%. Again, these results show that the second set of the frequencies had the lowest error (0.02%) in mesh convergence, and this implies that

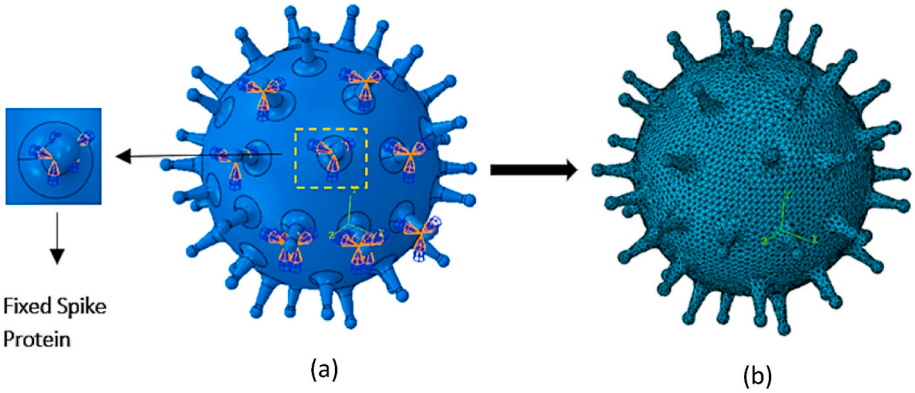

Fig. 2. Simulated SARS-CoV-2 model developed using Abaqus. (a) The initial model demonstrated 8 fixed spikes, (b) the second model shows the meshed model with a seed part of 1.5.

the frequency set met the resonance in the second case.

Based on this initial assessment, involving different numbers of fixed spike proteins of SARS-CoV-2, the natural frequency value ranging from 88.974 MHz to 125.126 MHz were obtained depending on the number of spike proteins considered from the mesh convergence error. The mesh convergence error of the eigenvalues of 21 were more converged compared to the other eigenvalues of 7 and 100. Hence, the error values were of 0.01%, 0.09% and 0.02%, all respectively. This demonstrated that the natural frequencies of the eigenvalues of 21 were closer to one another in contrast to the eigenvalues of 7 and 100 for all fixed spike proteins number of 6, 7 and 8.

4.4. Natural frequency and mode shapes

The equation of motion for a multiple degree of freedom system (MDoF) was introduced and used during the modal analysis for solving the natural frequencies of SARS-CoV-2. In this analysis, the mode values were referred to as eigenvalues and mode shapes were referred to as eigenvectors. Considering that the virus is an encastre selection of linear elasticity (U1=U2=U3=UR1 = UR2 = UR3 = 0) (Mia et al., 2017), the equation of motion for MDoF can be written as:

$$m\ddot{x} + c\dot{x} + kx = F(t) \tag{2}$$

where m is the mass matrix, $\ddot{x}$ is the acceleration vector, c is the damping matrix, $\dot{x}$ is the velocity vector, k is the stiffness matrix, x is the displacement vector and $F(t)$ is the external vector of excitation.

In addition, the system was considered as undamped as the virus has no energy losses when attached to the host cell as opposed to when replicating, so the second term in equation (2) can be deleted, resulting in:

$$m\ddot{x} + kx = F(t) \tag{3}$$

The equation of motion was transformed into an algebraic equation where $F(t)$ was equal to zero to solve for the natural frequencies and mode shapes.

$$m\ddot{x} + kx = 0 \tag{4}$$

An assumption for x was then made, where u present mode shapes:

$$x = \{u\}e^{-i\omega t} \tag{5}$$

By differentiating and substituting the assumed x value back to equation (4), the natural frequencies and mode shapes of the system were obtained. This can be done using the Modal Expansion Theorem of a superposition of a response of each natural modes of the system (Colun, 2018).

$$\left[-\omega^2 m + k\right]ue^{-i\omega t} = 0 \tag{6}$$

Since mode shapes u are generally not equal to zero hence the determinant of MDoF matrix $[-\omega^2 m + k]$ should equate to zero which then allows to obtain two sets of natural frequencies:

$$\left[-\omega^2\begin{bmatrix} M_1 & 0 & 0 \\ 0 & M_2 & 0 \\ 0 & 0 & M_3 \end{bmatrix} + \begin{bmatrix} K_1 & -K_1 & 0 \\ -K_1 & K_1+K_2 & -K_2 \\ 0 & -K_2 & K_2+K_3 \end{bmatrix}\right] = \begin{Bmatrix} 0 \\ 0 \\ 0 \end{Bmatrix} \tag{7}$$

By incorporating the values obtained in Table 1 for the stiffness (k) and mass (m) in equation (7), where: $k = K1 = K2 = K3 = 13 \times 10^{-3}$ N/m and $m = M1 = M2 = M3 = 1.6605 \times 10^{-18}$ kg, the two natural frequencies were obtained. Inserting these natural frequencies into equation (6) gave the modes information as shown in equations (8) and (9).

$$\begin{matrix} \text{Frequencies:} \\ 88.52\ MHz, \\ 125.13\ MHz\ and \\ 168.54\ MHz \end{matrix} \tag{8}$$

$$\text{Mode shapes } (u): \left[\begin{Bmatrix} 1.0000 \\ 0.8019 \\ 0.4450 \end{Bmatrix}\begin{Bmatrix} 1.0000 \\ -0.55 \\ -1.2470 \end{Bmatrix}\begin{Bmatrix} 1.0000 \\ -2.2470 \\ 1.8019 \end{Bmatrix}\right] \tag{9}$$

The frequencies found through this theoretical computation reflect just the three mode shapes. Note that the frequencies corresponding to the modal analysis simulation represented 100 mode shapes. Hence, frequencies obtained in this theoretical study were merely an example validating the frequencies of the simulation with the theoretical for mode 1 and 2 and were 88.52 and 125.13 MHz, respectively. The theoretical frequency for mode shape 3 was not considered as one of the final frequencies did not appear in the simulation for 100 mode shapes for all different fixed spike proteins.

Interpretation from the mode shapes u from the system indicated movement of mode 1 (1.0000) by 1 unit vertically, which caused the other two values in mode 1 to move by 0.8019 and 0.4450 times in the same positive direction (frequency amplitude wave). However, in mode 2, when the upper value moved 1.0000 unit, the other two bottom values moved in the opposite y-axis direction, as they had a negative sign, which was equivalent to a mode value of phase angle of 180° and amplitude of 0.555 times on the second value and 1.2470 times on the third value. The highest frequency amplitude waveform for all mode shapes 1 and 2 were of 1.0000.

4.5. Behaviour of mode shapes

An inverse of mode shape u, equation (10), was solved to obtain the response of the modal coordinates and transient decay of the system for mode shape 1 and 2.

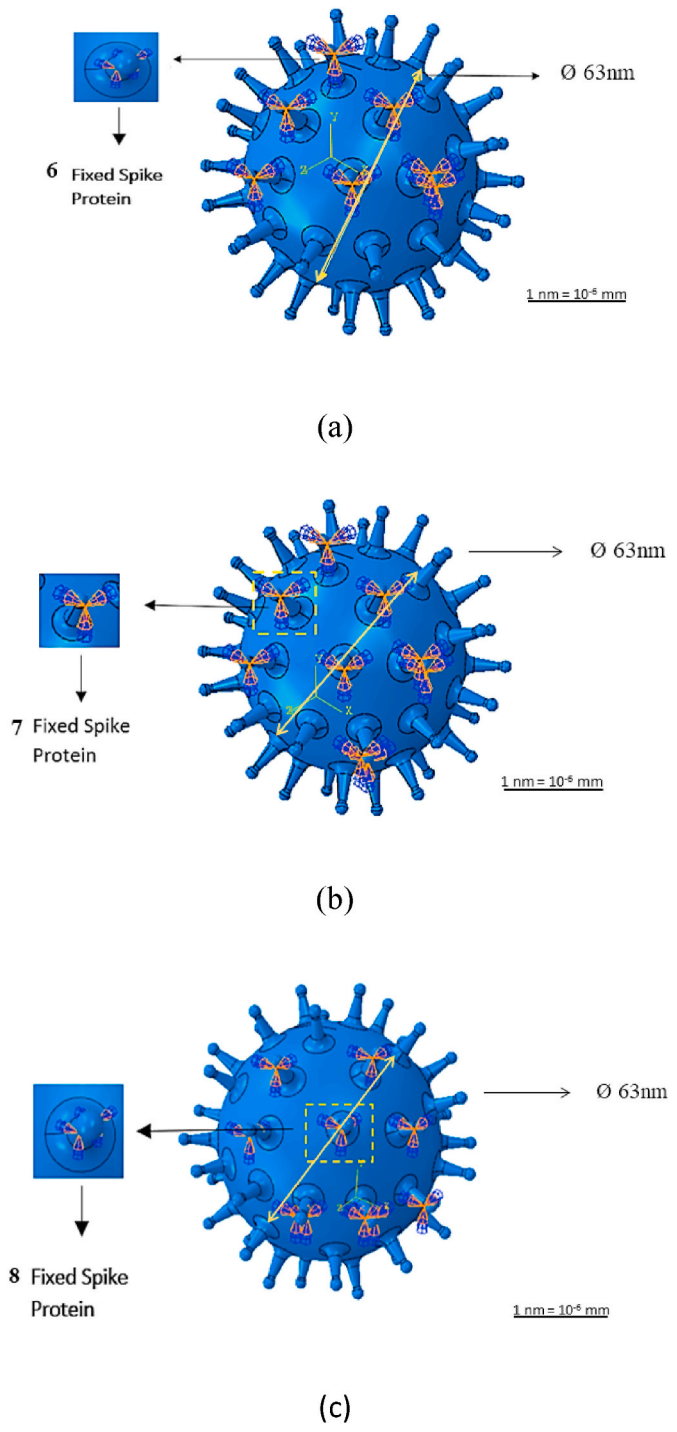

Fig. 3. 3D model of SARS-CoV-2 with a central height of 63 nm (a) shows 6 fixed spike proteins (BC). (b) shows 7 fixed spike proteins and (c) shows 8 fixed spike proteins to replicate the virus attachment to cell.

$$\text{Mode shape } (u): \quad \left[\begin{Bmatrix} 1.0000 \\ 0.8019 \\ 0.4450 \end{Bmatrix} \begin{Bmatrix} 1.0000 \\ -0.55 \\ -1.2470 \end{Bmatrix}\right] \tag{10}$$

$$\text{Inverse mode shape (u): } u^{-1} = \frac{1}{det(u)} x\, adj(u) \tag{11}$$

$$u^{-1} = \left[\begin{Bmatrix} 0.5431 \\ 0.3492 \\ 0.1075 \end{Bmatrix} \begin{Bmatrix} 0.4355 \\ -0.55 \\ -1.2470 \end{Bmatrix}\right]$$

Fig. 4 shows the inverse mode shapes value response to their natural frequency, with a minimum frequency of 88.52 MHz for mode shape 1 $\begin{Bmatrix} 0.5431 \\ 0.3492 \\ 0.1075 \end{Bmatrix}$ and a maximum frequency of 125.13 MHz for mode shape 2 $\begin{Bmatrix} 0.4355 \\ -0.55 \\ -1.2470 \end{Bmatrix}$.

In mode shape 1, mode 1 (0.5431), the oscillation amplitude was the largest compared to mode 2 (0.3492) and 3 (0.1075), which made the initial deflection mainly located in mode 1 due to its value in amplitude being the greatest. $(q_{1,2,3})$ here was the modal coordinate.

$$\text{Mode shape } 1 : x_0 = \begin{Bmatrix} 1 \\ 0 \\ 0 \end{Bmatrix} \rightarrow \begin{Bmatrix} 0.5431 \\ 0.3492 \\ 0.1075 \end{Bmatrix} = \begin{Bmatrix} q_1 \\ q_2 \\ q_3 \end{Bmatrix} \tag{12}$$

However, when the unit deflection (x) was located in mode 2 of value 1, it can be seen that the second and third modal coordinate (q_{2_0}) and (q_{3_0}) of mode 2 and 3 had a negative amplitude with respect to mode 1. These negative amplitudes were the effect of the unit deflection located in mode 2, implying that mode 2 had an impact on mode 3 vibration direction.

$$x = \begin{Bmatrix} 0 \\ 1 \\ 0 \end{Bmatrix} \rightarrow \begin{Bmatrix} 0.4355 \\ -0.1938 \\ -0.2411 \end{Bmatrix} = \begin{Bmatrix} q_1 \\ q_2 \\ q_3 \end{Bmatrix} \tag{13}$$

Therefore, the SARS-CoV-2 modal analysis provided a method to define the fundamental dynamic characteristics of this system. The exercise was pursued mathematically to compute natural frequencies, mode shapes and modal coordinates to create a mathematical model for its dynamic behaviour. The eigenvalues obtained from the modal analysis was for the 7, 21 and 100 of each of the last 7 values. Moreover, based on the decayed values, vibrational speed and their velocity in modal coordinate regarding their oscillation amplitude, mode 1 was then referred as lateral bending and mode 2 as torsion. Hence, these names mathematically summarised their dynamic characteristic.

5. Remarks on whether the frequency can harm a human being

The use of radio frequency has been used for centuries by many cosmetic doctors to help cure skin problems such as loose skin, body sculpting and many more other effective treatments (Ratini, 2021). However, the exposure of high radio frequency on human body is known to heat the biological tissue because of the body's inability to cope with or dissipate the excessive heat, leading to potential causes of cancer (FCC, 2022). It is important to differentiate the maximum permissible radio frequency which can be applied to human body without damaging any body parts. As such, the maximum permissible exposure to radio frequency on human body were developed from the recommendations of two expert organizations: the National Council on Radiation Protection (NCRP) and the Institute of Electrical and Electronics Engineers (IEEE). From the guideline provided by these two organizations, the most restrictive limits on whole-body exposure are in the frequency range of 30–300 MHz where the human body absorbs radio frequency energy most efficiently when the whole body is exposed (FCC, 2022). Hence,

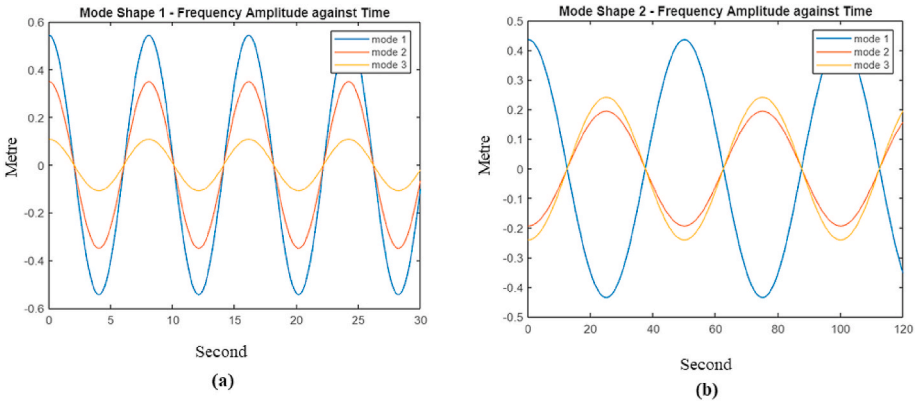

Fig. 4. Mode shapes 1 and 2 oscillations with their respective frequencies. The value inputs were obtained from the inverse mode shape (u) matrix. (a) is the results for the natural frequency of 88.52 MHz and (b) for the natural frequencies of 125.13 MHz.

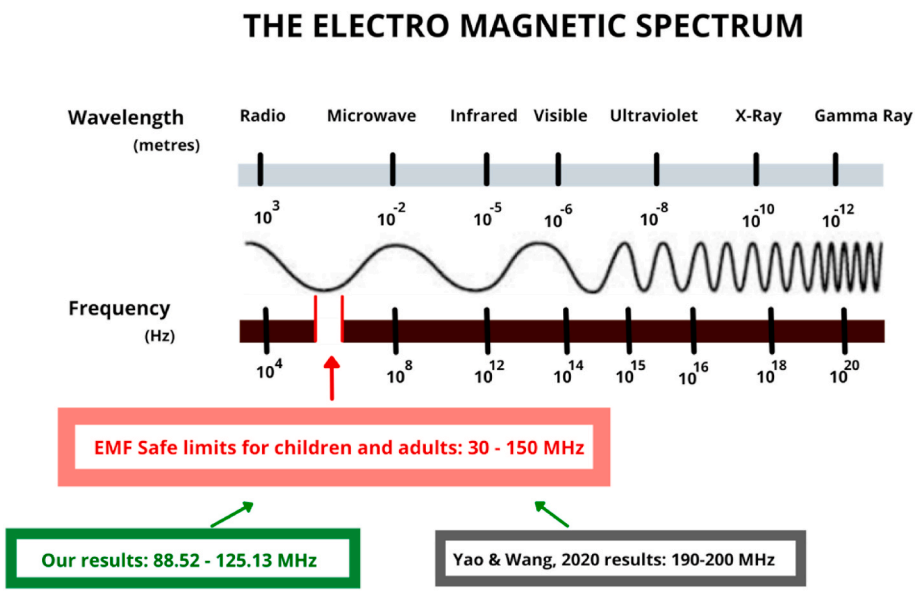

Fig. 5. EM spectrum depicting the frequency and wavelength ranges characterised by Radio, microwave, IR, Visible, UV, Xray and Gamma rays. Our research result is shown in green where it is within the safe limit recommended by EMF for adults and children, as well as the results found by Yao & Wang is within the frequencies found in our study.

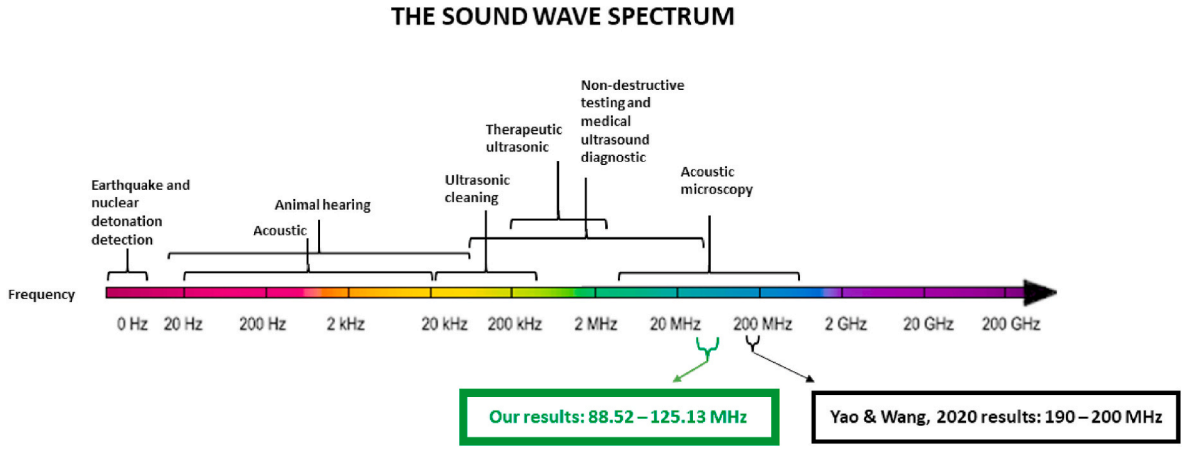

Fig. 6. Sound wave spectrum. The sound wave spectrum depicting the frequency characterised by Radio, Microwave, Earthquake and nuclear detonation detection, Acoustic, Animal hearing, Ultrasonic cleaning, Therapeutic ultrasonic, Non-destructive testing and medical ultrasound diagnostic and Acoustic microscopy. Our research results is shown in green between the range used for non-destructive testing and medical ultrasound diagnostic and the acoustic microscopy. The results found by Yao & Wang is also within the frequency limit of the acoustic microscopy.

particular care will be required when using electromagnetic waves in this range. These are mapped on the electromagnetic spectrum shown in Fig. 5.

It is also reported by the EMF-Portal (EMF-PORTAL, 2018), that the resonance range for maximum absorption for adults is in the region of 30–100 MHz, for instance for a body height of 1.80 m, the frequency field is about 83.3 MHz, whereas for children, the resonant frequency is higher due to their smaller size and it is reported that the maximum absorption for a body height of 1 m is about 150 MHz. Additionally, a key factor to consider is the posture of a human body, e.g., standing, sitting or lying, as this influences the whole-body absorption of radio frequency fields in the resonance range. The penetration depth of radio frequency field in body tissue also plays an important role on the level of safety to humans depending on the frequency and tissue type (such as brain, muscle, fat, kidney, skin and bones yellow/red bone marrow). In the results obtained from our FEA, the natural frequencies found for the SARS-CoV-2 were between a minimum of 88.52 and a maximum of 125.13 MHz, respectively (i.e. corresponding to about 0.1 GHz as in the EMF-Portal). The penetration depth at such frequency is about 2.7 cm in kidney and muscle tissues, about 3.9 cm in brain, skin and red bone marrow, about 14 cm in fat and 30 cm in bones and yellow bone marrow. Although, the frequency range obtained in the FEA exceeds the resonant frequencies in the human body, which is below 20 MHz (Yao and Wang, 2020), there is a possibility for such resonance frequency range to be applied on the human body by means of ultrasound wave rather than electromagnetic (EM) waves, so that it could be exploited in ultrasound medical devices. Fig. 6 highlights our results mapped across a range of frequencies used industrially. Frequency ranging from 0.5 MHz to 100 MHz are typically used for practical medical applications including imaging, physiotherapy, and focused ultrasonic surgery. Frequency above 100 MHz becomes distinct from frequencies between 0.5 and 100 MHz due to the beam-widths which is sufficiently narrow that limits heating, whilst retaining local forces (Leighton, 2018). This separates application at high frequencies compared to lower frequencies for medical applications. It was reported by (Leighton, 2018) that at frequency of 0.5 MHz, the wavelength in soft tissue is approximately 3 mm and at 100 MHz it is about 0.015 mm. Additionally, the ultrasound absorption in soft tissue follows an approximately linear frequency dependence with a typical absorption coefficient of about 0.5 dB cm^{-1} MHz^{-1}. Thus, the half-power thickness at 0.5 MHz is about 12 cm, comparable with the dimensions of a large organ such as the liver or the brain. Contrarily, the half power thickness at 100 MHz is only 0.06 cm which is comparable to the geometry of a tissue (Leighton, 2018). It suggests that applying frequencies in the range of 88.52 MHz–100 MHz within what we have numerically predicted can be regarded as safe to use for medical application.

Additionally, the resonant frequency from 88.52 MHz to 125.13 MHz could be used even on objects (not only on humans) to destroy the SARS CoV-2 virus on various types of surfaces. The known nanoscale data obtained from AFM, which was fed to the FEA in this work could have a lot of variances, due to the nature of the virus itself. Therefore, this theoretical study is only providing a basis to show what is feasible, but experimental efforts following from this simulation would ensure whether the obtained frequency is safe to use and whether they denature the virus instantly.

6. Conclusions

This paper presents a new aspect on investigating the modal characteristics of SARS-CoV-2 using finite element analysis and identifying the safe range to use natural frequencies on human beings. This paper actively contributes to the current gap in understanding the dynamic behaviour of SARS-CoV-2 and reports a novel and sustainable way by which microbes can be denatured without aggravating the problem of antimicrobial resistance (AMR). Based on the aforementioned discussions, the following broad conclusions can be drawn:

1. Based on the FEA model for a 63 nm diameter virus with different numbers of fixed spike proteins of 6, 7 and 8 for modal analysis, a linear time-invariant vibratory system was analysed. The Frequency Response Functions were described through an intricate mathematical function due to the modal analysis ability to decompose these complex mathematical values into a set of decouple single degree of freedom systems to compute different mode shapes. These mode shapes represent a reference of either deformation or vibration which can be excited at their natural frequency. Moreover, the SARS-CoV-2 modal analysis provided a method for defining the fundamental dynamic characteristics of this system.
2. A significant result obtained from this study was the finding of the range of natural frequencies that would denature SARS-CoV-2 by applying an external frequency. This frequency range was found to be in the range of 88.52–125.13 MHz. The suitable method that can be used to destroy such virus is by using a standing or laying full rotation excitation, which would result in denaturing the virus structure upon rotation around the human body using ultrasound or electromagnetic waves which could be exploited in different medical devices. Additionally, besides the possible direct application on the human body, this method could also represent an effective and safe route to sterilize the surfaces of environments and objects without the use of any chemical substance.
3. This feasibility study based on the simulations demonstrates that the SARS-CoV-2 can be denatured at a safe penetration depth level and frequency which could possibly not affect human health, although a field trial involving in-vitro testing is strongly recommended before applying or using this method on living beings.

CRediT authorship contribution statement

Caaisha Warsame: Visualization, Writing – original draft. **Daniele Valerini:** Formal analysis, Writing – review & editing. **Iñigo Llavori:** Formal analysis. **Asa H. Barber:** Writing – review & editing. **Saurav Goel:** Supervision, Funding acquisition, Conceptualization, Writing Writing – review & editing review & editing.

Declaration of competing interest

The authors declare that they have no known competing financial interests or personal relationships that could have appeared to influence the work reported in this paper.

Data availability

Data will be made available on request.

Acknowledgements

SG greatly acknowledge the financial support provided by the UKRI via Grants No. EP/S036180/1, EP/T001100/1 and EP/T024607/1″ and feasibility study awards from the ‘Transforming Foundation Industries NetworkPlus (EP/V026402/1), the UKRI National Interdisciplinary Circular Economy Hub (EP/V029746/1). We also acknowledge the generous funding support from the Royal Academy of Engineering via Grants No. IAPP18-19\295 and TSP1332, EURAMET EMPIR A185 (2018), Alliance Hubert-Curien Mobility award from the British Council and the Newton Fellowship award from the Royal Society (NIF\R1 \191571). The work made use of Isambard Bristol, UK supercomputing service accessed by a Resource Allocation Panel (RAP) grant as well as ARCHER2 resources (Project e648).

Appendix 1

Table 2
Frequency values obtained from mesh convergence of SARS-CoV-2 with 6 fixed spike proteins (BC). These frequencies were obtained when 7, 21 and 100 eigenvalues were compared.

Frequencies (Hz) of the last 7 values		
Eigenvalue of 7	Eigenvalue of 21	Eigenvalue of 100
57.1208946E+06	88.97438E+06	99.32414E+06
59.0042332E+06	88.97661E+06	100.54738E+06
9.227838E+06	88.98136E+06	100.67593E+06
9.635691E+06	88.98545E+06	101.06382E+06
9.646282E+06	88. 98569E+06	101.73893E+06
10.326621E+06	88. 98577E+06	102.00354E+06
86.54681E+06	88. 98630E+06	102.28744E+06
Mesh Convergence		
Error of 34%	Error of 0.01%	Error of 2.17%

Appendix 2

Table 3
Frequency value obtained from mesh convergence of SARS-CoV-2 with 7 fixed spike proteins (BC). These frequencies were obtained when 7, 21 and 100 eigenvalues were compared.

Frequencies (Hz) of the last 7 values		
Eigenvalue of 7	Eigenvalue of 21	Eigenvalue of 100
37.3799829E+06	112.08096E+06	148.21765E+06
29.6311232E+06	112.08233E+06	151.76371E+06
34.9583577E+06	112.10544E+06	153.32315E+06
35.0065111E+06	112.15439E+06	155.68590E+06
36.5436784E+06	112.16790E+06	155.98432E+06
62.06930E+06	111.17378E+06	161.00987E+06
91.17069E+06	112.18138E+06	167.12266E+06
Mesh Convergence		
Error of 59%	Error of 0.09%	Error of 11.31%

Appendix 3

Table 4
Frequency value obtained from mesh convergence of SARS-CoV-2 with 8 fixed spike proteins (BC). These frequencies were obtained when 7, 21 and 100 eigenvalues were compared.

Frequencies (Hz) of the last 7 values		
Eigenvalue of 7	Eigenvalue of 21	Eigenvalue of 100
77.06399E+06	125.09331E+06	157.23488E+06
77.45450E+06	125.09386E+06	158.01589E+06
79.58572E+06	125.11415E+06	159.12654E+06
839.8319E+06	125.11438E+06	159.48767E+06
941.0936E+06	125.11612E+06	160.39691E+06
122.26982E+06	125.12645E+06	160.50392E+06
124.29677E+06	125.12677E+06	160.85601E+06
Mesh Convergence		
Error of 38%	Error of 0.02%	Error of 2.25%

References

Abaqus, D., 2012. Natural Frequency Extraction. https://abaqus-docs.mit.edu/2017/English/SIMACAEANLRefMap/simaanl-c-freqextraction.htm.

Arbely, E., Khattari, Z., Brotons, G., Akkawi, M., Salditt, T., Arkin, I.T., 2004. A highly unusual palindromic transmembrane helical hairpin formed by SARS coronavirus E protein. J. Mol. Biol. 341 (3), 769–779. https://doi.org/10.1016/j.jmb.2004.06.044.

Colun, J., 2018. Mode Superposition. Retrieved from. https://www.comsol.com/multiphysics/mode-superposition.

Dastjerdi, S., Malikan, M., Akgöz, B., Civalek, Ö., Wiczenbach, T., Eremeyev, V.A., 2022. On the deformation and frequency analyses of SARS-CoV-2 at nanoscale. Int. J. Eng. Sci. 170, 103604 https://doi.org/10.1016/j.ijengsci.2021.103604.

EMF-PORTAL, 2018. Radio Frequency (10 MHz-300GHz). Retrieved from. https://www.emf-portal.org/en/cms/page/home/effects/radio-frequency.

FCC, 2022. RF Safety FAQ. Retrieved from. https://www.fcc.gov/engineering-technology/electromagnetic-compatibility-division/radio-frequency-safety/faq/rf-safety.

Goel, S., Hawi, S., Goel, G., Thakur, V.K., Agrawal, A., Hoskins, C., Barber, A.H., 2020. Resilient and agile engineering solutions to address societal challenges such as coronavirus pandemic. Mater. Today Chem. 17, 100300 https://doi.org/10.1016/j.mtchem.2020.100300.

Huang, Y., Yang, C., Xu, X.-f., Xu, W., Liu, S.-w., 2020. Structural and functional properties of SARS-CoV-2 spike protein: potential antivirus drug development for COVID-19. Acta Pharmacol. Sin. 41 (9), 1141–1149. https://doi.org/10.1038/s41401-020-0485-4.

Ivanovska, I.L., de Pablo, P.J., Ibarra, B., Sgalari, G., MacKintosh, F.C., Carrascosa, J.L., Wuite, G.J., 2004. Bacteriophage capsids: tough nanoshells with complex elastic properties. Proc. Natl. Acad. Sci. U. S. A. 101 (20), 7600–7605. https://doi.org/10.1073/pnas.0308198101.

Jiang, S., Hillyer, C., Du, L., 2020. Neutralizing antibodies against SARS-CoV-2 and other human coronaviruses. Trends Immunol. 41 (5), 355–359. https://doi.org/10.1016/j.it.2020.03.007.

Ke, Z., Oton, J., Qu, K., Cortese, M., Zila, V., McKeane, L., Briggs, J.A.G., 2020. Structures and distributions of SARS-CoV-2 spike proteins on intact virions. Nature 588 (7838), 498–502. https://doi.org/10.1038/s41586-020-2665-2.

Kiss, B., Kis, Z., Pályi, B., Kellermayer, M.S.Z., 2021. Topography, spike dynamics, and nanomechanics of individual native SARS-CoV-2 virions. Nano Lett. 21 (6), 2675–2680. https://doi.org/10.1021/acs.nanolett.0c04465.

Leighton, F.D.a.T., 2018. Frequency bands for ultrasound, suitable for the consideration of its health effects. J. Acoust. Soc. Am. 144 (4) https://doi.org/10.1121/1.5063578.

Lyonnais, S., Henaut, M., Neyret, A., Merida, P., Cazevieille, C., Gros, N., Muriaux, D., 2021. Atomic force microscopy analysis of native infectious and inactivated SARS-CoV-2 virions. Sci. Rep. 11 (1), 11885 https://doi.org/10.1038/s41598-021-91371-4.

Mia, M.S., Islam, M.S., Ghosh, U., 2017. Modal analysis of cracked cantilever beam by finite element simulation. Procedia Eng. 194, 509–516. https://doi.org/10.1016/j.proeng.2017.08.178.

Neuman Benjamin, W., Adair Brian, D., Yoshioka, C., Quispe Joel, D., Orca, G., Kuhn, P., Buchmeier Michael, J., 2006. Supramolecular architecture of severe Acute respiratory Syndrome coronavirus revealed by electron cryomicroscopy. J. Virol. 80 (16), 7918–7928. https://doi.org/10.1128/JVI.00645-06.

Peddieson, J., Buchanan, G.R., McNitt, R.P., 2003. Application of nonlocal continuum models to nanotechnology. Int. J. Eng. Sci. 41 (3), 305–312. https://doi.org/10.1016/S0020-7225(02)00210-0.

Raamsman, M.J., Locker, J.K., de Hooge, A., de Vries, A.A., Griffiths, G., Vennema, H., Rottier, P.J., 2000. Characterization of the coronavirus mouse hepatitis virus strain A59 small membrane protein E. J. Virol. 74 (5), 2333–2342. https://doi.org/10.1128/jvi.74.5.2333-2342.2000.

Ratini, M., 2021. What is radiofrequency skin tightening? Retrieved from. https://www.webmd.com/beauty/what-is-radiofrequency-skin-tightening#:~:text=It%20is%20a%20popular%20treatment,of%20the%20genitals%20without%20surgery.

Sally, R., 2020. Researchers Try and Pop SARS-CoV-2 with an AFM Tip - Virion Surprisingly Resilient. Retrieved from. https://www.news-medical.net/news/20200920/Researchers-try-and-pop-SARS-CoV-2-with-an-AFM-tip-virion-surprisingly-resilient.aspx.

Stephanidis, B., Adichtchev, S., Gouet, P., McPherson, A., Mermet, A., 2007. Elastic properties of viruses. Biophys. J. 93 (4), 1354–1359. https://doi.org/10.1529/biophysj.107.109033.

Tachibana, M., Koizumi, H., Kojima, K., 2004. Effect of intracrystalline water on longitudinal sound velocity in tetragonal hen-egg-white lysozyme crystals. Phys. Rev. E - Stat. Nonlinear Soft Matter Phys. 69 (5 Pt 1), 051921 https://doi.org/10.1103/PhysRevE.69.051921.

Tai, W., He, L., Zhang, X., Pu, J., Voronin, D., Jiang, S., Du, L., 2020. Characterization of the receptor-binding domain (RBD) of 2019 novel coronavirus: implication for development of RBD protein as a viral attachment inhibitor and vaccine. Cell. Mol. Immunol. 17 (6), 613–620. https://doi.org/10.1038/s41423-020-0400-4.

Turoňová, B., Sikora, M., Schürmann, C., Hagen, W.J.H., Welsch, S., Blanc, F.E.C., Beck, M., 2020. In situ structural analysis of SARS-CoV-2 spike reveals flexibility mediated by three hinges. Science 370 (6513), 203–208. https://doi.org/10.1126/science.abd5223.

Venkatagopalan, P., Daskalova, S.M., Lopez, L.A., Dolezal, K.A., Hogue, B.G., 2015. Coronavirus envelope (E) protein remains at the site of assembly. Virology 478, 75–85. https://doi.org/10.1016/j.virol.2015.02.005.

Wierzbicki, T., Li, W., Liu, Y., Zhu, J., 2021. Effect of receptors on the resonant and transient harmonic vibrations of Coronavirus. J. Mech. Phys. Solid. 150, 104369 https://doi.org/10.1016/j.jmps.2021.104369.

Yao, M., Wang, H., 2020. A potential treatment for COVID-19 based on modal characteristics and dynamic responses analysis of 2019-nCoV. Nonlinear Dynam. 1–8. https://doi.org/10.1007/s11071-020-06019-1.